01 Sep 2022

Processing and Mechanical Properties of Hot-Pressed Zirconium Diboride – Zirconium Carbide Ceramics

Eric W. Neuman

William Fahrenholtz
Missouri University of Science and Technology, billf@mst.edu

Gregory E. Hilmas
Missouri University of Science and Technology, ghilmas@mst.edu

Recommended Citation

E. W. Neuman et al., "Processing and Mechanical Properties of Hot-Pressed Zirconium Diboride – Zirconium Carbide Ceramics," *Journal of the European Ceramic Society*, vol. 42, no. 11, pp. 4472 - 4478, Elsevier, Sep 2022.
The definitive version is available at https://doi.org/10.1016/j.jeurceramsoc.2022.04.053

Journal of the European Ceramic Society 42 (2022) 4472–4478

Contents lists available at ScienceDirect

Journal of the European Ceramic Society

journal homepage: www.elsevier.com/locate/jeurceramsoc

Processing and mechanical properties of hot-pressed zirconium diboride – zirconium carbide ceramics

Eric W. Neuman [*,1], William G. Fahrenholtz, Gregory E. Hilmas

Materials Science and Engineering Department, Missouri University of Science and Technology, Rolla, MO 65409, USA

ARTICLE INFO

Keywords:
Zirconium diboride
Zirconium carbide
Hot-pressing
Mechanical properties

ABSTRACT

ZrB_2 was mixed with 0.5 wt% carbon and up to 10 vol% ZrC and densified by hot-pressing at 2000 °C. All compositions were > 99.8% dense following hot-pressing. The dense ceramics contained 1–1.5 vol% less ZrC than the nominal ZrC addition and had between 0.5 and 1 vol% residual carbon. Grain sizes for the ZrB_2 phase decreased from 10.1 μm for 2.5 vol% ZrC to 4.2 μm for 10 vol% ZrC, while the ZrC cluster size increased from 1.3 μm to 2.2 μm over the same composition range. Elastic modulus was ~505 GPa and toughness was ~2.6 MPa·$m^{½}$ for all compositions. Vickers hardness increased from 14.1 to 15.3 GPa as ZrC increased from 2.5 to 10 vol%. Flexure strength increased from 395 MPa for 2.5 vol% ZrC to 615 MPa for 10 vol% ZrC. Griffith-type analysis suggests ZrB_2 grain pullout from machining as the strength limiting flaw for all compositions.

1. Introduction

Structural materials capable of withstanding temperatures in excess of 2000 °C for extended periods are critical for the development of hypersonic airframe and propulsion components. Zirconium diboride is of interest for such applications due to its high melting temperature (3245 °C), low density (6.09 g/cm^3), high thermal conductivity, oxidation resistance, and high strength [1]. The borides generally exhibit higher thermal conductivities and lower electrical resistivities at room temperatures than carbide and nitride ceramics [2,3]. Borides also show good resistance to chemical attack [4]. These properties have made borides candidates for applications including refractory linings [5,6], molten metal crucibles [7,8], furnace electrodes [7], cutting tools [4,9], and especially for use on future hypersonic aerospace vehicles [10,11].

Most research on ZrB_2 based ceramics has focused on either ZrB_2-SiC or ZrB_2-$MoSi_2$ compositions. These materials have exhibited good room temperature properties, with strengths exceeding 1000 MPa and fracture toughness values exceeding 5 MPa·$m^{½}$ [12,13]. However, both of these materials have chemical stability issues that limit the use temperature to below 2000 °C. Specifically, the ZrB_2-SiC system has a eutectic at 2270 °C and the melting point of $MoSi_2$ is 2030 °C. The ZrB_2-ZrC_x system is promising for use above 2000 °C, as its eutectic occurs between 2660 °C and 2830 °C, depending on the ZrC stoichiometry [14,15].

The properties of borides that lend themselves well to high temperature applications also make densification difficult. Historically, temperatures in excess of 2200 °C along with applied pressures on the order of tens of MPa were required to densify diborides [1]. More recent research has lowered the densification temperature of zirconium diboride. Chamberlain et al. was able to achieve 99.8% dense ZrB_2 following hot pressing at 1900 °C, a result of reducing the starting particle by attrition milling [12]. Chamberlain et al. later showed that the same procedure could be used to produce 98.0% dense ZrB_2 by pressureless sintering [16]. The densification was enhanced by the reduction of the starting ZrB_2 particle size from 2 μm to 0.5 μm, isothermal holds that promoted removal of surface oxides, and the introduction of tungsten carbide (WC) into the powder by wear of the grinding media. The surfaces of ZrB_2 powder particles are covered with a layer of native oxides, specifically ZrO_2 and B_2O_3, which promote coarsening and inhibit densification. Removal of these oxides is needed to promote solid state densification mechanisms. The B_2O_3 can be removed using isothermal holds under mild vacuum. For example, the equilibrium vaporization point of B_2O_3 liquid under mild vacuum (~20 Pa) occurs at 1340 °C [17,18]. Hence, isothermal holds during the hot pressing cycle can be used to remove B_2O_3. The ZrO_2 is more persistent, but can be removed by reaction with additives such as carbon, boron carbide, or tungsten carbide [18–21]. For example, in the pressureless

* Correspondence to: P.O. Box 5800, Albuquerque, NM 87185-0963, USA.
E-mail address: neumane@mst.edu (E.W. Neuman).
[1] Present address: Sandia National Laboratories, Albuquerque, Mexico.

https://doi.org/10.1016/j.jeurceramsoc.2022.04.053
Received 7 April 2022; Accepted 26 April 2022
Available online 29 April 2022

Table 1
Summary of nominal and actual batching amounts, theoretical density, bulk density, and relative density for the ZrB_2-ZrC ceramics hot-pressed at 2000 °C.

Sample ID	Nominal ZrC Addition (vol%)	Batched Amounts (wt%)				Theoretical Density (g/cm^3)	Bulk Density (g/cm^3)	Relative Density (%)
		ZrB_2	ZrC	C	Media Erosion			
ZZC025	2.5	93.36	2.60	0.49	3.55	6.143	6.133 ± 0.012	99.83
ZZC050	5.0	88.07	5.01	0.46	6.46	6.155	6.148 ± 0.001	99.88
ZZC075	7.5	87.70	7.67	0.46	4.16	6.166	6.164 ± 0.002	99.96
ZZC100	10.0	86.08	10.30	0.45	3.17	6.178	6.174 ± 0.001	99.94

Table 2
Summary of phase ZrC and C phase composition for the ZrB_2-ZrC ceramics hot-pressed at 2000 °C.

Sample ID	Phase Composition (vol%)		
	ZrC		Carbon
	Image Analysis	XRD	Image Analysis
ZZC025	0.96 ± 0.29	0.5 ± 0.2	0.79 ± 0.24
ZZC050	3.22 ± 0.28	3.4 ± 0.2	1.11 ± 0.36
ZZC075	6.57 ± 0.49	5.8 ± 0.2	0.51 ± 0.08
ZZC100	8.86 ± 0.96	8.3 ± 0.2	0.89 ± 0.17

sintering reported by Chamberlain, WC enhanced densification of ZrB_2 by reacting with ZrO_2 on the surface of the particles and removing the oxygen in the form of CO gas.

Investigations into the effect of zirconium carbide (ZrC) additions on the densification of ZrB_2 have been limited. Gropyanov et al. showed that additions of ZrC to ZrB_2 improved densification [22]. They showed that additions of 10 vol% ZrC lowered the activation energy for sintering by ~25% and suppressed grain growth. Andrievskii et al. hot pressed ZrB_2-5 vol% ZrC and achieved ~5 vol% porosity after hot pressing at 2200 °C [23]. They also found that the addition increased the grain size of the ZrB_2 phase from 13 μm to 27 μm for similar hot pressing conditions. Kats et al. showed that 20 vol% additions of ZrC into ZrB_2 reduced the porosity from 10.6% to 2.9%, and reduced the grain size of the ZrB_2 from 6 to 8 μm to 2–4 μm after hot pressing at 2100 °C. More recently, Tsuchida et al. used spark plasma sintering to produce a 97.5% dense compact of ZrB_2-20 vol% ZrC at 1800 °C [24]. Most other recent work investigating additions of ZrC to ZrB_2 based materials has focused on ternary ZrB_2-SiC-ZrC[25–27] and ZrB_2-$MoSi_2$-ZrC compositions [28].

Microstructure plays a critical role in the failure of brittle materials. Watts et al. related the effect of SiC particle size to the mechanical properties of ZrB_2-SiC.[29] Thermal residual stresses that built up during cooling from the densification temperature lead to compressive stresses in the SiC phase and tensile stresses in the ZrB_2 phase. Watts determined that the strength of the ceramics decreased gradually with maximum SiC particle size until ~11.5 μm, at which point a dramatic decrease in strength occurred due to spontaneous matrix microcracking. Similar results are expected to occur in ZrB_2 ceramics that exhibit mismatches between the coefficients of thermal expansion (CTEs) of the constituent phases.

The purpose of the research reported herein was to design a two-phase particulate reinforced microstructure with a low volume fraction reinforcing phase with desirable mechanical properties. The manuscript will discuss the processing and mechanical properties of zirconium diboride ceramics with up to 10 vol% additions of zirconium carbide.

2. Experimental procedure

2.1. Processing

Commercially available ZrB_2 powder (Grade B, H. C. Starck, Karlsruhe, Germany) and ZrC powder (Grade A, H. C. Starck), were the starting materials. A soluble phenolic resin (GP 2074, Georgia Pacific, Atlanta, GA) was added as a carbon precursor (~43 wt% C yield at 800 °C in Ar/10 H_2) to react with and remove surface oxides. Powders were dispersed in 2-butanone by ball milling for 8 h with a dispersant (DISPERBYK®−110, BYK-Gardner USA, Columbia, MD) using ZrB_2 media.[2] Phenolic resin was added to the mixture and milled for an additional 16 hr. Contamination from media erosion was 1.02 ± 0.02 wt %. Following ball milling, the slurry was dried by rotary evaporation (Model Rotavapor R-124, Buchi, Flawil, Germany) at a temperature of 70 °C, low vacuum (~27 kPa), and a rotation speed of 120 rpm. The dried powders were lightly ground to pass through a 50-mesh screen prior to hot-pressing.

Milled powders were hot-pressed (Model HP20–3060–20, Thermal Technology, Santa Rosa, CA) in 44.5 mm circular graphite dies lined with BN coated (SP-108, Cerac, Milwaukee, WI) graphite foil (2010-A, Mineral Seal Corp., Tucson, AZ). Prior to hot pressing, the powders were cold compacted in a uniaxial press at ~2 MPa. Powder compacts were pyrolyzed by heating at 5 °C/min under flowing Ar/10H2 to a 1 h isothermal hold at 800 °C. Following charring, the furnace was evacuated, then heated under vacuum (~13 Pa) to 1250 °C with an average heating rate of 10 °C/min. After holding for 2 h, the temperature was increased to 1450 °C at an average heating rate of 10 °C/min. Following a 2 h hold, the temperature was increased to 1600 °C at an average heating rate of 10 °C/min. After 1 h, the furnace was back filled with Ar/10H2 and a uniaxial load of 32 MPa was applied. Following previous studies, the isothermal holds were used to promote reactions between surface oxides on the starting powders and carbon to remove the oxides as gaseous species [18,30]. The furnace was then heated at ~20 °C/min to 1900 °C. After 45 min, the furnace was cooled at a rate of 20 °C/min. The load was removed when the die temperature dropped below 1600 °C.

During hot-pressing, the change in thickness of the specimens was measured in-situ using a linearly variable differential transducer (LVDT) attached to the hot-press rams. The effect of linear thermal expansion of the rams and load train during heating to process temperatures on the calculated densities was corrected using the ram displacement measured during cooldown from the process temperature. Time-dependent density values were calculated using Eq. (1):

$$\rho_i = \rho_f \left(1 + \frac{L_i - \alpha_{HP}(T_f - T_i)}{L_f}\right) \quad (1)$$

where L_f is the final length, L_i is the change in length at time i, α_{HP} is the measured CTE of the hot-press load train, T_f is the maximum furnace temperature, T_i is the furnace temperature at time i, and ρ_f is the final density. The instantaneous densification rate was calculated using a step-wise numerical process from the measured ram displacement [Eq. (2)]:

$$\dot{\rho}_i = \frac{1}{\rho_i}\frac{(\rho_i - \rho_{i-1})}{(t_i - t_{i-1})} \quad (2)$$

[2] Fabricated using ZrB_2 with additions of 1 wt% B_4C and 1 wt% C (phenolic source), ball milled with WC-6Co (~1 wt% added to powder through erosion). Uniaxially pressed into cylinders (0.5 in D x 0.5 in H), cold isostatically pressed, then pressurelessly sintered at 2050 °C for 90 min in flowing Ar/H_2.

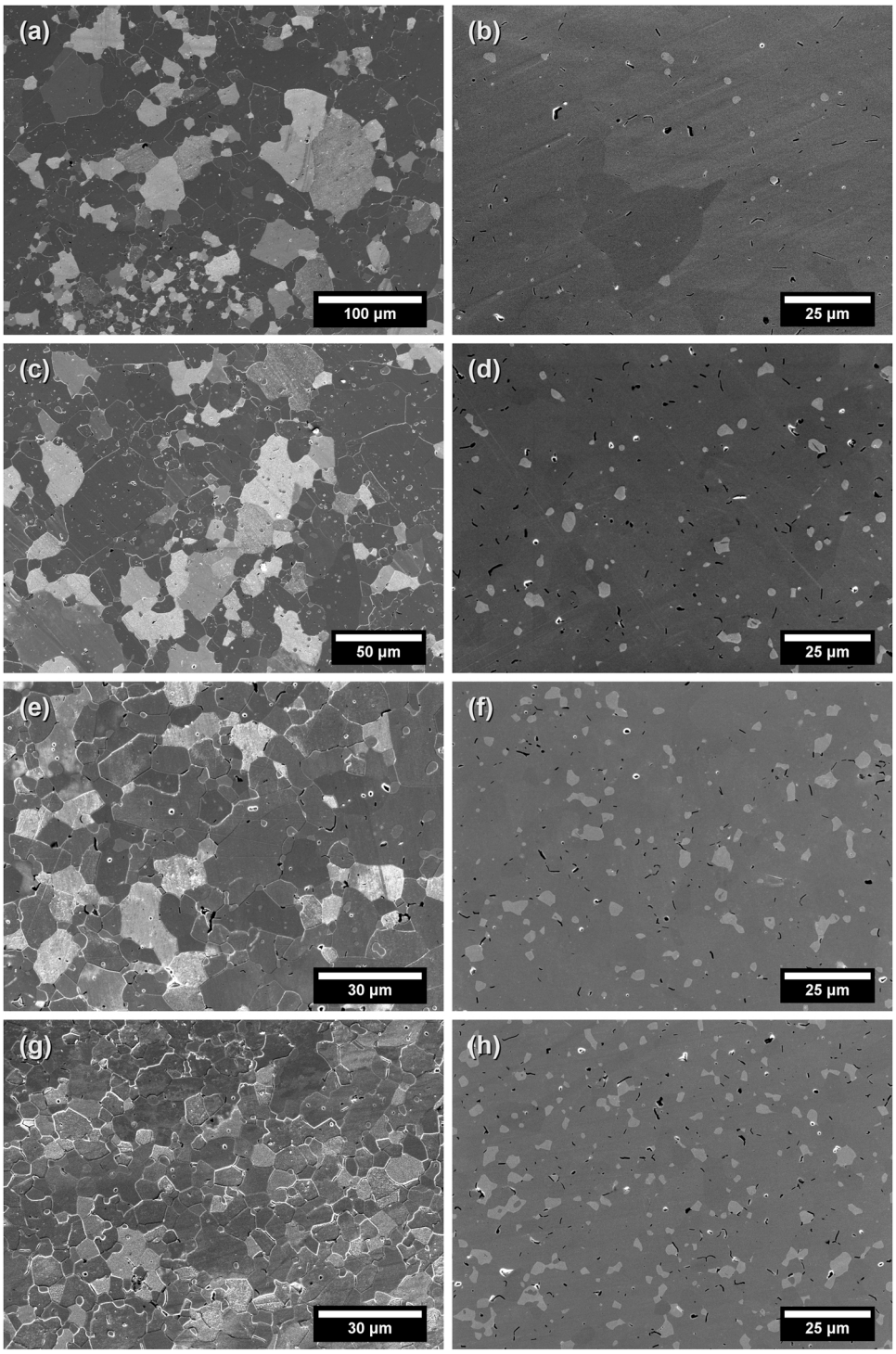

Fig. 1. Chemically etched (left) and polished (right) cross sections of ZrB_2-ZrC ceramics hot pressed at 2000 °C with 2.5 (a, b), 5.0 (c, d), 7.5 (e, f), and 10 vol% ZrC (g, h).

where ρ_i is the relative density at time i, and t_i is time i. The calculated instantaneous densification rate was smoothed using 6 point weighted adjacent averaging with repeated boundary conditions (OriginPro 2021, OriginLab Corp., Northampton, MA).

2.2. Characterization

Bulk density of the pressurelessly sintered specimens was measured by Archimedes' method using distilled water as the immersing medium according to ASTM C373. Specimens were prepared for density measurement by hand grinding the surface of the pellets on a 15 µm diamond polishing pad. Relative density was calculated by dividing the Archimedes' density by the density predicted from the nominal compositions of ZrB_2, ZrC, C and milling media erosion. Microstructures were examined using scanning electron microscopy (SEM; Helios NanoLab 600, FEI, Hillsboro, OR) with simultaneous chemical analysis by energy dispersive spectroscopy (EDS; Oxford Instruments, Abingdon, UK). Specimens were prepared for microscopy by cutting cross sections perpendicular to the uniaxial pressing direction and polishing to a

Table 3
Summary of the grain size and shape descriptors for the ZrB_2, ZrC, and C phases in the ZrB_2-ZrC ceramics hot-pressed at 2000 °C.

Phase	Sample ID	Grain Size (μm)			Aspect Ratio
		Equivalent Area Diameter	Major Ellipse	Maximum Major Ellipse	
ZrB_2	ZZC025	10.1 ± 9.9	13.1 ± 13.3	130.9	1.7 ± 0.6
	ZZC050	9.2 ± 8.9	11.8 ± 12.2	114.4	1.7 ± 0.6
	ZZC075	5.3 ± 3.9	6.7 ± 5.1	56.4	1.7 ± 0.7
	ZZC100	4.2 ± 2.4	5.2 ± 3.4	22.7	1.6 ± 0.5
ZrC	ZZC025	1.3 ± 0.9	1.7 ± 1.2	6.81	1.5 ± 0.5
	ZZC050	1.8 ± 1.1	2.2 ± 1.4	9.30	1.6 ± 0.6
	ZZC075	2.2 ± 1.3	2.7 ± 1.8	11.4	1.6 ± 0.5
	ZZC100	2.2 ± 1.3	2.8 ± 1.9	14.5	1.7 ± 0.6
Carbon	ZZC025	0.7 ± 0.4	1.4 ± 1.0	7.1	2.8 ± 1.4
	ZZC050	0.7 ± 0.3	1.2 ± 0.8	5.8	2.4 ± 1.2
	ZZC075	2.1 ± 1.3	0.8 ± 0.8	7.2	2.7 ± 1.5
	ZZC100	2.2 ± 1.3	1.1 ± 0.8	5.5	2.7 ± 1.3

0.25 μm finish using successively finer diamond abrasives. The ZrB_2 was etched using molten KOH at 200 °C for ~2 s. ZrB_2 and ZrC grain size was manually measured from SEM images of the polished and etched cross-section using a digitizer and image editing software (Photoshop CS5, Adobe Systems, San Jose, CA), as well as image analysis software (ImageJ 1.50 f, National Institutes of Health, Bethesda, MA), and is reported as the equivalent projected area diameter (EAD). The grain size distribution of the ZrB_2 phase, and the cluster size distribution of the ZrC phase, were estimated by fitting ellipses to at least 500 grains, or clusters, respectively.

2.3. Mechanical testing

Room temperature flexure strengths were measured in four-point bending using a fully-articulated test fixture using type-A bars (25 mm × 2.0 mm×1.5 mm) according to ASTM C1161–02c. Ten specimens were tested at room temperature and five specimens were tested at each elevated temperature. Bars were machined from the hot-pressed billets by diamond grinding on a fully automated surface grinder (FSG-3A818, Chevalier, Santa Fe Springs, CA) using a 600-grit diamond grinding wheel and chamfered by hand using 15 μm diamond abrasives. Tests were performed using a screw-driven instrumented load frame (Model 5881, Instron, Norwood, MA) and a deflectometer was used to record bar displacement. Elastic modulus was determined using the static bend test method according to ASTM standard E111. A minimum of five measurements were averaged to calculate the reported values. Hardness was measured by Vickers indentation following ASTM C1327 (Duramin 5, Struers Inc., Cleveland, OH), with an indentation load of 9.81 N and a dwell time of 15 s. Fracture toughness was measured utilizing the direct crack method (DCM) described by Anstis et al. [31] A Vickers diamond indenter (V-100-A2, LECO Corp., St. Joseph, MI) was used with an indentation load of 98.1 N and a dwell time of 15 s; the resulting indent was measured using an optical light stage microscope (Epiphot 200, Nikon, Tokyo, Japan). A minimum of ten measurements were averaged to calculate the reported mechanical property values.

3. Results and Discussion

Measured bulk densities for the hot-pressed specimens ranged from 6.13 to 6.17 g/cm^3 for nominal ZrC additions of 2.5–10 vol%, respectively (Table 1). The calculated theoretical densities for the compositions are also shown in Table 1, assuming 6.15 g/cm^3 for ZrB_2 based on the reported Hf content of the powder (1.9 wt%),[32] 6.56 g/cm^3 for the ZrC,[33] and 6.167 g/cm^3 for the ZrB_2 milling media.[32] The amounts of secondary phase were also determined following hot-pressing by image analysis and XRD (Table 2). Minimal porosity was observed in all specimens. Hence, all compositions were > 99.8% dense.

SEM micrographs showing both the polished and chemically etched microstructures can be seen in Fig. 1. The measured grain size and shape descriptors for the ZrB_2, ZrC, and C phases observed in the hot-pressed microstructures are summarized in Table 3. From the etched microstructures, the addition of 2.5 and 5.0 vol% ZrC resulted in abnormal

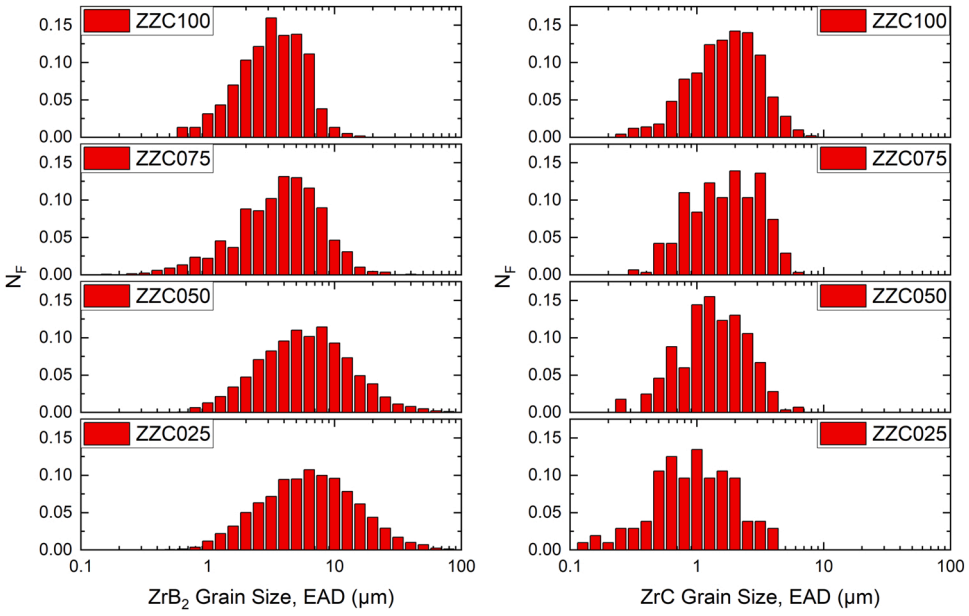

Fig. 2. Cumulative ZrB_2 (left) and ZrC (right) grain size distributions for ZrB_2-ZrC ceramics hot pressed at 2000 °C. Please note the log scale for the grain size.

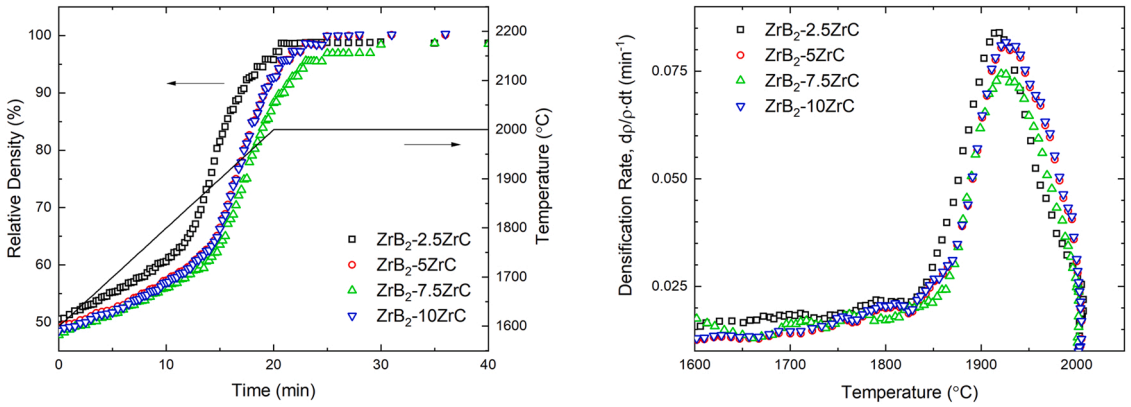

Fig. 3. Density as a function of sintering time (left) and densification rate as a function of temperature (right) for ZrB_2-ZrC ceramics hot pressed at 2000 °C.

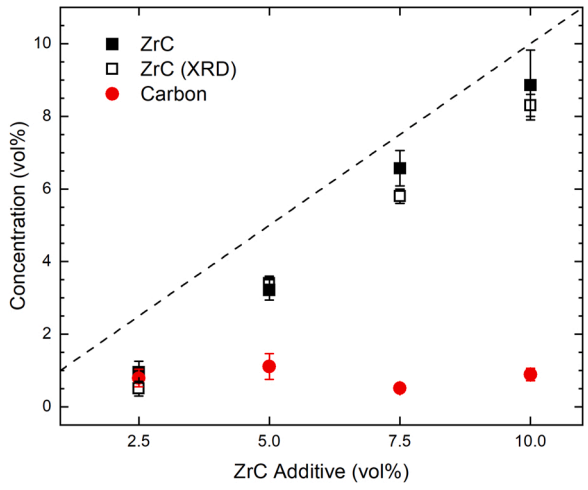

Fig. 4. ZrC and carbon concentrations following hot pressing for ZrB_2-ZrC ceramics hot pressed at 2000 °C. Dashed line represents the batched ZrC concentration.

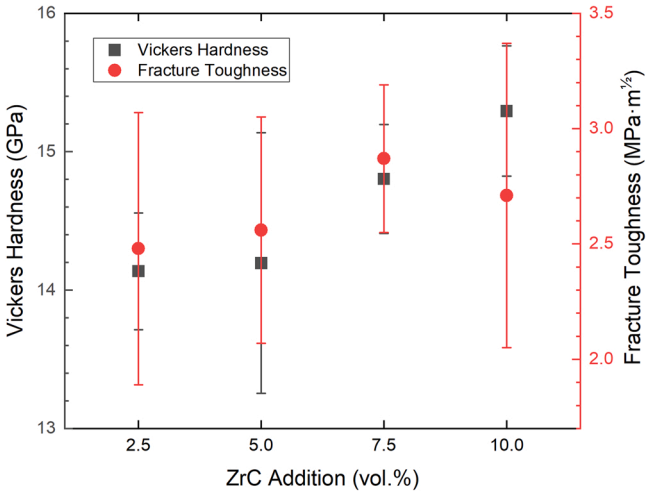

Fig. 5. Vickers hardness (black squares) and fracture toughness (red circles) as a function of ZrC additive for the ZrB_2-ZrC ceramics hot pressed at 2000 °C.

Table 4
Summary of elastic modulus, Vickers hardness, fracture toughness, and flexure strength for the ZrB_2-ZrC ceramics hot-pressed at 2000 °C.

Sample ID	Elastic Modulus (GPa)	$HV_{0.5,\ 15\ s}$ (GPa)	Fracture Toughness ($MPa{\cdot}m^{1/2}$)	Flexure Strength (MPa)
ZZC025	510 ± 10	14.1 ± 0.4	2.5 ± 0.6	396 ± 40
ZZC050	495 ± 8	14.2 ± 0.9	2.6 ± 0.5	426 ± 64
ZZC075	508 ± 14	14.8 ± 0.4	2.9 ± 0.3	503 ± 31
ZZC100	506 ± 5	15.3 ± 0.5	2.7 ± 0.7	613 ± 24

grain growth of the ZrB_2 phase with some ZrB_2 grains reaching ~130 μm. Increasing the addition of ZrC to 7.5 and 10 vol% resulted in finer microstructures, and no abnormal grain growth was observed. The volume weighted cumulative grain size distribution for ZrB_2 is given in Fig. 2, and shows that additions of 2.5 and 5.0 vol% ZrC resulted in a few large (Dv50, > ~40 μm) ZrB_2 grains that comprise the bulk of the microstructure, with numerous small (Dn50, < ~5 μm) ZrB_2 grains. Additions of ZrC of 7.5 vol% or 10 vol% suppressed the growth of the ZrB_2 grains, likely through a grain pinning mechanism, and shifted the grain size distribution to finer and more uniform grain sizes.

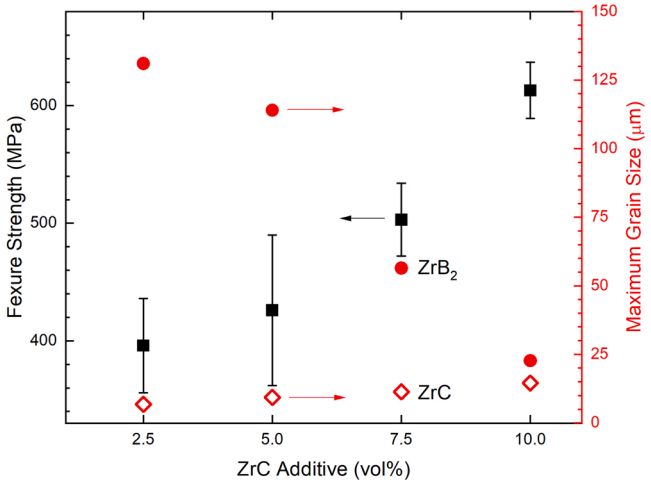

Fig. 6. Flexure strength (black squares) and maximum ZrB_2 (red circles) and ZrC (red diamonds) grain size as a function of ZrC additive for ZrB_2-ZrC ceramics hot pressed at 2000 °C.

Importantly, the maximum grain size observed in the ZrB_2 phase decreases with increasing amounts of ZrC. Both the average and maximum ZrC clusters size also increased with increasing ZrC concentration

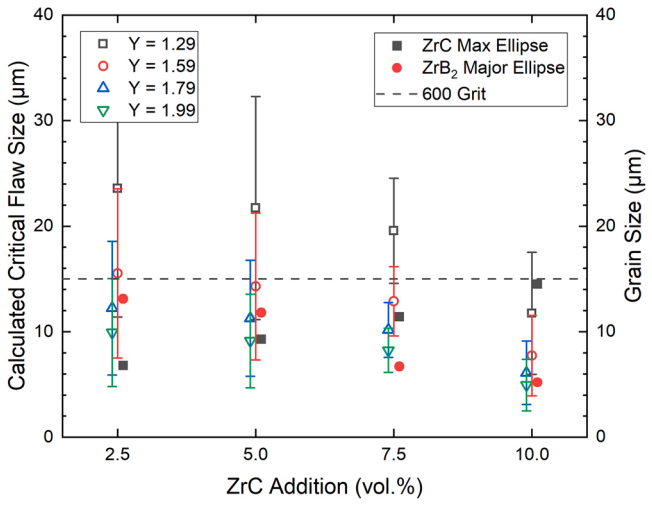

Fig. 7. Calculated Griffith critical flaw as a function of ZrC addition. The ZrC maximum major ellipse grain size, ZrB_2 average major ellipse grain size, and nominal 600 grit abrasive size are shown for comparison.

(Fig. 2). Average ZrC size increased from 1.3 μm for 2.5 vol% ZrC to 2.2 μm for 10 vol% ZrC addition, while the maximum ZrC cluster size increased from 6.8 to 14.5 μm over the same range.

Densification curves are shown in Fig. 3. Full density was reached soon after beginning the isothermal hold at 2000 °C. The densification rate is also shown in Fig. 3 as a function of the furnace temperature during heating under load. The maximum densification rate occurred at temperatures between 1910 °C and 1930 °C. Since the temperature in the hot-press is measured from the outside of the die wall, the temperature of the powder compact may be lower that the reported temperature, but the maximum densification rate occurs at approximately 1900 °C.

The compositions of the ceramics following hot pressing was determined using x-ray diffraction (XRD), Raman spectroscopy, and image analysis (Fig. 4). XRD identified ZrB_2 and ZrC as the only crystalline phases following hot pressing. Rietveld refinement of the XRD patterns, along with aerial analysis, was used to determine the amount of ZrC present. Aerial analysis was also used to determine the amount of a third, low Z-contrast phase present. The low Z-contrast phase was identified as graphitic carbon by Raman spectroscopy. The amount of ZrC in the final ceramics was ~1.5 vol%, less than expected based on the amounts added (assuming a ZrB_2 density of 6.15 g/cm^3 and a ZrC density of 6.56 g/cm^3). Further, approximately 1 vol% of residual carbon was present for all ZrC additive concentrations. A previous study that used 0.5 wt% carbon as a sintering aid found that no residual carbon was observed following hot pressing.[34] The excess carbon observed in the present study is attributed to carbon formed by decomposition of ZrC during densification.

The effect of the amount of ZrC additive on the elastic modulus, Vickers hardness, and flexure strength was determined (Table 4). The elastic modulus was measured from the stress-strain response as 510 ± 10 GPa for 2.5 vol% ZrC, 495 ± 8 GPa for 5.0 vol% ZrC, 508 ± 14 GPa for 7.5 vol% ZrC, and 506 ± 5 GPa for 10 vol% ZrC. A linear fit of the elastic modulus data finds a fit of $E = 501 + 0.4x$, where x is the nominal ZrC addition in vol%, with an R^2 of 0.06 and p-value of 0.76. This analysis suggests elastic modulus does not vary for this range of ZrC additions to ZrB_2 and that the elastic modulus is ~505 GPa for the ZrB_2-ZrC ceramics.

Using a load of 0.5 kg, Vickers hardness increased from 14.1 GPa for 2.5 vol% ZrC to 15.3 GPa for 10 vol% ZrC addition (Fig. 5). The increase in Vickers hardness followed the trend of $HV = 13.7 + 0.153x$, where x is the nominal ZrC addition in vol%, having an R^2 of 0.97 and p-value of 0.018, significant at the standard $\alpha = 0.05$ level. Fracture toughness also increased from 2.5 MPa·m$^{1/2}$ for 2.5 vol% ZrC to 2.7 MPa·m^{½} for 10 vol % ZrC (Fig. 5). The linear fit to the data results in $K_{IC} = 2.37 + 0.06x$, with an R^2 of 0.58 and p-value of 0.24, indicating that the observed increase was not statistically significant.

The flexure strength (Fig. 6) increased from 395 MPa for 2.5 vol% ZrC additions to 615 MPa for 10 vol% ZrC additions. The one-way analysis of variance (ANOVA) for the strength as a function of ZrC addition finds $\sigma = 301 + 30x$, with an R^2 of 0.95 and p-value of 0.023, indicating statistical significance for increasing strength with increasing ZrC addition. The maximum ZrB_2 grain sizes and ZrC cluster sizes are also shown in Fig. 6, and shows that the flexure strength follows an inverse relation to the maximum ZrB_2 grain size. The maximum ZrC cluster size was significantly smaller (a factor of 5 or more) compared to the maximum ZrB_2 grain size for additions of 2.5, 5.0 and 7.5 vol% ZrC, and similar for additions of 10 vol% (ZrB_2, 22 μm; ZrC, 14 μm). The critical flaw sizes were estimated using a Griffith-type analysis (Fig. 7), utilizing the measured flexure strength and fracture toughness values in combination with geometric stress intensity factors ranging from Y = 1.29 (half-penny surface crack) to Y = 1.99 (long semi-elliptical surface crack). Fracture surfaces were not able to be imaged, as specimens typically fractured into multiple fragments upon failure during flexure testing. From the Griffith analysis, the largest ZrB_2 grains were not acting as the flaw, as these features are several times larger than the calculated critical flaws. While the largest ZrC sizes were within the range of the calculated critical flaw sizes, the size trends for ZrC particles progress in the opposite direction as the critical flaw size with increasing ZrC additions. Machining damage from the 600-grit abrasive used to prepare the specimens is also on the order of the critical flaw size, but if this were the critical flaw, the critical flaw size would be expected to be unchanging with ZrC addition. Instead, the average ZrB_2 grains track well with the calculated critical flaw sizes for semi-elliptical surface cracks (Y = 1.59–1.99). This behavior was previously reported and confirmed by fractography by Neuman et al. for similar ZrB_2 – 10 vol% ZrC ceramics [35]. The critical flaws in the study by Neuman were reported as machining induced surface damage characterized by zipper cracks on the order of the larger ZrB_2 grains, though not the largest ZrB_2 grains. In the present ceramics, it is thus likely that a similar mechanism occurred and that the critical flaws are a combination of ZrB_2 grain pullout and zipper cracks from specimen machining.

4. Summary

ZrB_2 ceramics with additions of ZrC between 2.5 and 10 vol% were prepared by hot-pressing. The powders were prepared by ball milling with ZrB_2 grinding media to minimize contamination from media erosion, and 0.5 wt% carbon was added to react with and remove surface oxides on the powder. All ceramics were > 99.8% dense following hot-pressing. SEM and XRD analysis showed that ZrC contents in the final ceramics were approximately 1–1.5 vol% less than expected based on the nominal ZrC additions. In addition, all compositions had between 0.5 and 1 vol% residual carbon. Grain size for the ZrB_2 phase decreased from 10.1 μm for the 2.5 vol% ZrC addition to 4.2 μm for the 10 vol% ZrC addition. Across the same composition range, the ZrC cluster size increased from 1.3 μm to 2.2 μm. Elastic modulus was ~505 GPa for the compositions. Vickers hardness increased from 14.1 to 15.3 GPa as the ZrC addition increased from 2.5 to 10 vol%. The direct crack fracture toughness increased slightly, from 2.5 to 2.7 MPa·m^{½} with increasing ZrC addition. Flexure strength increased from 395 MPa for 2.5 vol% ZrC addition to 615 MPa for 10 vol% ZrC addition. A Griffith-type analysis suggests that ZrB_2 grain pullout or machining induced damage from specimen preparation are likely the strength limiting flaws in the present study.

Declaration of Competing Interest

The authors declare that they have no known competing financial

interests or personal relationships that could have appeared to influence the work reported in this paper.

Acknowledgements

The authors would like to thank Ashley Hilmas, Lucas Showalter, Conner Wittmaier, and John Tomaszewski for their assistance with the production of the ZrB_2 grinding media and specimen preparation. We would also like to the Advanced Materials Characterization Laboratory at Missouri S&T for their assistance with specimen characterization. Research at Missouri S&T was supported by the High Temperature Aerospace Materials Program (Dr. Ali Sayir, program manager) at the Air Force Office of Scientific Research through grant FA9550-09-1-0168.

References

[1] W.G. Fahrenholtz, G.E. Hilmas, I.G. Talmy, J.A. Zaykoski, Refractory diborides of zirconium and hafnium, J. Am. Ceram. Soc. 95 (5) (2007) 1347–1364.
[2] M. Rahman, C.C. Wamg, W. Chen, S.A. Akbar, C. Mroz, Electrical resistivity of titanium diboride and zirconium diboride, J. Am. Ceram. Soc. 78 (5) (1995) 1380–1382.
[3] J.W. Zimmerman, G.E. Hilmas, W.G. Fahrenholtz, R.B. Dinwiddie, W.D. Porter, H. Wang, Thermophysical properties of ZrB_2 and ZrB_2-SiC ceramics, J. Am. Ceram. Soc. 91 (5) (2008) 1405–1411.
[4] S.K. Mishra, S.K. Das, P. Ramachandrarao, Sintering studies on ultrafin ZrB_2 powder produced by a self-propagating high-temperature synthesis process, J. Mater. Res 15 (11) (2000) 2499–2504.
[5] Kuwabara K., Skamoto S., Kida O., Ishino T., Kodama T., Nakajima T., et al. Corrosion Ressistance and Electrical Resistivity of ZrB2 Monolithic Refractories. The Proceedings of UNITECT 2003,. 2003:The 8th Biennial Worldwide Conference on Refractories.
[6] N. Kaji, H. Shikano, I. Tanaka, Developement of ZrB_2-graphite protective sleeve for submerged nozzle, Taikabutsu Overseas 14 (2) (1992) 39–43.
[7] Z.J. Jin, M. Zhang, D.M. Guo, R.K. Kang, Electroforming of copper/ZrB_2 composite coating and performance as eltron-discharge machining electrodes, Key Eng. Mater. 291–292 (2005) 537–542.
[8] J. Sung, D.M. Goedde, G.S. Girolami, J.R. Abelson, Remote-plasma chemical vapor deposition of conformal ZrB_2 films at low temperature: a promissing diffusion barrier for ltralarge scale integrated electronics, J. Appl. Phys. 91 (6) (2002) 3904–3911.
[9] Murata Y. Cutting Tool Tips and Ceramics Containing Hafnium Nitride and Zirconium Diboride. U. S. Patent No 3,487,594. 1970.
[10] A.L. Chamberlain, W.G. Fahrenholtz, G.E. Hilmas, Low-temperature densification of zirconium diboride ceramics by reactive hot pressing, J. Am. Ceram. Soc. 89 (12) (2006) 6368–6375.
[11] M.M. Opeka, I.G. Talmy, J.A. Zaykoski, Oxidation-based materials selection for 2000°C + hypersonice aerosurfaces: theoretical considerations and historical experience, J. Mater. Sci. 39 (19) (2004) 5887–5904.
[12] A.L. Chamberlain, W.G. Fahrenholtz, G.E. Hilmas, High-strength zirconium diboride-based ceramics, J. Am. Ceram. Soc. 87 (6) (2004) 1170–1172.
[13] A.L. Chamberlain, W.G. Fahrenholtz, G.E. Hilmas, D.T. Ellerby, Characterization of zirconium diboride-molybdenum disilicide ceramics, in: N.P. Bansal, J.P. Singh, W. M. Kriven, H. Schneider (Eds.), Advances in Ceramic Matrix Composites IX, The American Ceramic Society, Westerville, OH, 2003, pp. 299–308.
[14] E. Rudy, S. Windisch, Part II: Ternary Systems: Volume XIII: Phase Diagrams of the Systems Ti-B-C, Zr-B-C, and Hf-B-C, Air Force Materials Laboratory, Wright-Patterson Air Force Base, OH, 1966, pp. 1–212.
[15] S.S. Ordan'yan, V.I. Unrod, Reactions in the system ZrC-ZrB_2, Sov. Powder Metall. Met. Ceram. 14 (5) (1975) 393–395.
[16] A.L. Chamberlain, W.G. Fahrenholtz, G.E. Hilmas, Pressureless sintering of zirconium diboride, J. Eur. Ceram. Soc. 89 (2) (2006) 450–456.
[17] W.G. Fahrenholtz, The ZrB_2 volatility diagram, J. Am. Ceram. Soc. 88 (12) (2005) 3509–3512.
[18] S.C. Zhang, G.E. Hilmas, W.G. Fahrenholtz, Pressureless densification of zirconium diboride with boron carbide additions, J. Am. Ceram. Soc. 89 (5) (2006) 1544–1550.
[19] A.L. Chamberlain, W.G. Fahrenholtz, G.E. Hilmas, Pressureless sintering of zirconium diboride, J. Am. Ceram. Soc. 89 (2) (2006) 450–456.
[20] W.G. Fahrenholtz, G.E. Hilmas, S.C. Zhang, S. Zhu, Pressureless sintering of zirconium diboride: particle size and additive effects, J. Am. Ceram. Soc. 91 (5) (2008) 1398–1404.
[21] W.G. Fahrenholtz, G.E. Hilmas, R. Li, Densification of ultra-refractory transition metal diboride ceramics, Sci. Sinter. 52 (1) (2020) 1–14.
[22] V.M. Gropyanov, L.M. Bel'tyukova, Sintering and recrystallization of ZrC-ZrB_2 compacts, Sov. Powder Metall. Met. Ceram. 7 (7) (1968) 527–533.
[23] R.A. Andrievskii, L.A. Korolev, V.V. Klimenko, A.G. Lanin, I.I. Spivak, I.L. Taubin, Effect of zirconium carbide and carbon additions on some physicomechanical properties of zirconium diboride, Sov. Powder Metall. Met. Ceram. 19 (2) (1980) 93–94.
[24] T. Tsuchida, S. Yamamoto, Spark plasma sintering of ZrB_2–ZrC powder mixtures synthesized by MA-SHS in air, J. Mater. Sci. 42 (3) (2007) 772–778.
[25] V. Medri, F. Monteverde, A. Balbo, A. Bellosi, Comparison of ZrB2-ZrC-SiC Composites Fabricated by Spark Plasma Sintering and Hot-Pressing, Adv. Eng. Mater. 7 (3) (2005) 159–163.
[26] Q. Qiang, Z. Xinghong, M. Songhe, H. Wenbo, H. Changqing, H. Jiecai, Reactive hot pressing and sintering characterization of ZrB_2–SiC–ZrC composites, Mater. Sci. Eng., A 491 (1) (2008) 117–123.
[27] W.W. Wu, G.J. Zhang, Y.M. Kan, P.L. Wang, Reactive hot pressing of ZrB_2–SiC–ZrC composites at 1600°C, J. Am. Ceram. Soc. 91 (8) (2008) 2501–2508.
[28] L. Silvestroni, D. Sciti, Microstructure and properties of pressureless sintered ZrC-based materials, J. Mater. Res 23 (7) (2008) 1882–1889.
[29] J. Watts, G. Hilmas, W.G. Fahrenholtz, Mechanical characterization of ZrB_2-SiC composites with varying SiC particle sizes, J. Am. Ceram. Soc. 94 (12) (2011) 4410–4418.
[30] S. Zhu, W.G. Fahrenholtz, G.E. Hilmas, S.C. Zhang, Pressureless sintering of zirconium diboride using boron carbide and carbon additions, J. Am. Ceram. Soc. 90 (11) (2007) 3660–3663.
[31] G. Anstis, P. Chantikul, B.R. Lawn, D. Marshall, A critical evaluation of indentation techniques for measuring fracture toughness. I.–Direct crack measurements, J. Am. Ceram. Soc. 64 (9) (1981) 533–538.
[32] E.W. Neuman, G.E. Hilmas, W.G. Fahrenholtz, Processing, microstructure, and mechanical properties of large-grained zirconium diboride ceramics, Mater. Sci. Eng. A 670 (2016) 196–204.
[33] P.T.B. Shaffer, Engineering properties of carbides, in: Jr.S.J.S. Schneider (Ed.), Ceramics and Glasses: Engineered Materials Handbook. 4, ASM International, Materials Park, OH, 1991, pp. 787–803.
[34] E.W. Neuman, G.E. Hilmas, W.G. Fahrenholtz, Strength of zirconium diboride to 2300°C, J. Am. Ceram. Soc. 96 (1) (2013) 47–50.
[35] E.W. Neuman, G.E. Hilmas, W.G. Fahrenholtz, Ultra-high temperature mechanical properties of a zirconium diboride-zirconium carbide ceramic, J. Am. Ceram. Soc. 99 (2) (2016) 597–603.